

Research Article

Microstructural Topology Optimization of Constrained Layer Damping on Plates for Maximum Modal Loss Factor of Macrostructures

Zhanpeng Fang , Lei Yao , Shuxia Tian, and Junjian Hou

Henan Engineering Research Center of New Energy Vehicle Lightweight Design and Manufacturing,
Zhengzhou University of Light Industry, Zhengzhou 450002, China

Correspondence should be addressed to Zhanpeng Fang; 2015073@zzuli.edu.cn and Lei Yao; 2016008@zzuli.edu.cn

Received 29 April 2020; Revised 10 September 2020; Accepted 24 September 2020; Published 13 October 2020

Academic Editor: Konstantin V. Avramov

Copyright © 2020 Zhanpeng Fang et al. This is an open access article distributed under the Creative Commons Attribution License, which permits unrestricted use, distribution, and reproduction in any medium, provided the original work is properly cited.

This paper presents microstructural topology optimization of viscoelastic materials for the plates with constrained layer damping (CLD) treatments. The design objective is to maximize modal loss factor of macrostructures, which is obtained by using the Modal Strain Energy (MSE) method. The microstructure of the viscoelastic damping layer is composed of 3D periodic unit cells. The effective elastic properties of the unit cell are obtained through the strain energy-based method. The density-based topology optimization is adopted to find optimal microstructures of viscoelastic materials. The design sensitivities of modal loss factor with respect to the design variables are analyzed and the design variables are updated by Method of Moving Asymptotes (MMA). Numerical examples are given to demonstrate the validity of the proposed optimization method. The effectiveness of the optimal design method is illustrated by comparing a solid and an optimized cellular viscoelastic material as applied to the plates with CLD treatments.

1. Introduction

Viscoelastic damping materials are desired in many engineering applications to reduce unwanted noise and vibration due to their favourable characteristics in dissipating dynamic energy. Damping treatment approaches including active, passive, and hybrid passive-active methods [1–3] have been developed to reduce noise and vibration and applied to many industrial fields. The constrained layer damping (CLD) treatments provide considerably more damping effect than unconstrained ones despite the addition of the additional weight of the constraining layer, and they are widely applied to attenuate the structural vibration. In order to design lightweight structures with high damping performance, the optimization for damping treatment has been extensively studied. Plunkett [4] proposed a method of cutting the constraining layer into appropriate lengths to increase the structure damping of the CLD structure. Ray

and Baz [5] studied the optimization of energy dissipation of active constrained layer damping treatments of plates. Nakra [6] investigated how to design the layout of CLD treatments to improve the vibration performance. Zheng et al. [7] proposed the layout optimization of the CLD treatments to minimize vibration energy and sound radiation of cylindrical shells.

Topology optimization method is regarded as a powerful tool for seeking innovative structural design. Bendsoe and Kikuchi [8] firstly proposed the topology optimization method by employing homogenization theory. With the development of the topology optimization method, several well-known topology optimization methods include the solid isotropic material with penalization (SIMP) method [9], level set method (LSM) [10], the Evolutionary Structural Optimization (ESO) [11], and the bidirectional evolutionary structural optimization (BESO) [12]. A series of methods for structural topology optimization were proposed to address

the layout problem of the damping layer in the past decades. Kim et al. [13] compared the modal loss factors of the structures with damping material treatment obtained by topology optimization to the ones obtained by other approaches and further demonstrated that topology optimization is the most effective way to find optimal damping layout in a shell structure. James and Waisman [14] proposed a time-dependent adjoint sensitivity analysis method to produce optimal designs of structures that exhibit viscoelastic creep deformation. Madeira et al. [15] optimized the distribution of CLD material on a laminated composite panel to minimize weight and maximize modal damping simultaneously.

The damping performance of CLD treatments mainly depends on the physical and geometric properties of the viscoelastic damping material. Therefore, there is a great desire to design the microstructures of viscoelastic materials with the demand property. Sigmund [16, 17] firstly proposed an inverse homogenization method to design materials with prescribed properties. Yi et al. [18] utilized the inverse homogenization method to optimize the microstructure of the damping material with the aim of improving the damping characteristics of viscoelastic composites. Huang et al. [19] utilized the BESO method to design the composite microstructure with the desirable viscoelastic properties. Liu et al. [20] proposed a topology optimization algorithm based on the BESO method to enhance the macroscopic modal damping and natural frequency of structures constructed by optimized viscoelastic materials.

Topology optimization problems involve a large number of design variables. Hence, gradient-based methods are preferred over evolutionary- and population-based approaches. It has been shown that, based on current computing technology, the evolutionary methods are prohibitively time- and resource-consuming for most reasonably sized topology optimization problems [21]. The Method of Moving Asymptotes (MMA) [22] is a well-known gradient-based algorithm, and it is widely used in topology optimization of structures. Zheng et al. [23] used topology optimization with MMA approach to optimally design damping treatment by maximizing damping effect. Kang et al. [24] investigated the optimal distribution of damping material in vibrating structures which subject to harmonic excitations by using a topology optimization method. El-Sabbagh and Baz [25] conducted topology optimization for unconstrained damping treatment of plates. Takezawa et al. [26] proposed complex dynamic compliance as objective function for optimizing damping materials to reduce the resonance peak response. Fang et al. [27] proposed an efficient optimization procedure integrating the Pseudoexcitation Method (PEM) and the double complex modal superposition method to optimize the layout of the CLD structures subjected to stationary random excitation. Chen and Liu [28] investigated the optimal microstructural configuration of the viscoelastic material to improve the damping characteristics of the macrostructures. Yun and Youn [29] optimized the microstructures of viscoelastic materials to effectively attenuate transient responses of the viscoelastic damping

structures. Zhao et al. [30] proposed an efficient concurrent topology optimization approach for minimizing the maximum dynamic response of two-scale hierarchical structures in the time domain.

Most of the present works concerning microstructural topology optimization of damping material has concentrated on the Sandwich beams. Microstructural topology optimization of damping material of a plate with CLD treatment is relatively limited. Therefore, the purpose of this paper is to optimize microstructure of viscoelastic material of the CLD plates with the aim of maximizing the modal loss factor of the macrostructure. The microstructure of the viscoelastic damping layer is represented by 3D periodical unit cell (PUC), and its effective shear modulus is obtained by using the strain energy-based method. The design sensitivities of modal loss factor with respect to the design variables are analyzed and the optimization problem is solved by the MMA approach.

2. Optimization Problem and Material Interpolation Scheme

A two-scale topology optimization problem of the CLD plate is studied in this paper. The macrostructure of the CLD plate is composed of the uniform cellular viscoelastic material. The microstructure of the viscoelastic damping layer is represented by 3D periodical unit cell. The optimization objective is to design the optimal layout of the viscoelastic material within the 3D periodical unit cell with the prescribed volume fraction so that the optimal CLD plate has a maximum modal loss factor for damping the vibration. Therefore, the optimization problem can be mathematically expressed as follows:

$$\left\{ \begin{array}{l} \text{find: } x_i, i = 1, 2, \dots, n, \\ \text{min: } -\eta_r (r = 1, 2, 3, \dots), \\ \text{s.t: } \frac{\sum_{i=1}^n x_i V_i}{\sum_{i=1}^n V_i} \leq V^*, \\ 0 < x_{\min} \leq x_i \leq 1, \quad i = 1, 2, \dots, n, \end{array} \right. \quad (1)$$

where x_i , $i = 1, 2, \dots, n$, are the design variables and n is the total number of the elements within the 3D periodical unit cell. $x_i = 1$ denotes that element i is full of viscoelastic damping material and $x_i = x_{\min}$ represents a void element. η_r is the r th mode loss factor. V_i is the volume of the i th element and V^* is the prescribed volume fraction.

The viscoelastic damping material of an element in the 3D periodical unit cell can be treated to be isotropic and its physical properties are assumed to be a function of the elemental density, x_i . To obtain relative clear 0-1 topological structure, the Solid Isotropic Material with Penalization (SIMP) model [31] with an exponential 'power-law' scheme is adopted to penalize the intermediate densities and the material interpolation scheme can be expressed as follows:

$$\begin{cases} \rho_i^v = x_i^q \rho^{v0}, \\ \mathbf{D}_i^{\text{mi}} = x_i^p (1 + j\eta^0) \mathbf{D}^{v0}, \end{cases} \quad (2)$$

where η^0 is the material loss factor and $j = \sqrt{-1}$. ρ^{v0} and \mathbf{D}^{v0} denote the density and the storage modulus of the viscoelastic damping material when $x_i = 1$. q and p are the penalty factors.

In the SIMP interpolation scheme, the reasonable penalty factor should be chosen to suppress the intermediate density elements in the final optimal topology. A small penalty factor will lead to a large number of intermediate density elements in the final optimal results as the punishment is insufficient in the process of solving. However, when the penalty parameter is too large, many high-relative-density elements (for example, greater than 0.5 and less than 1.0) may be irrational to delete. It will lead to checkerboard pattern numerical instability and even cause the incorrect optimization results [32]. The

combination of $q = 1$ and $p = 3$ is always used to optimize modal loss factor and vibration response [26–28, 33, 34]. Therefore, the penalty factors q and p are 1 and 3 in this paper.

3. Finite Element Analysis and Sensitivity Analysis

3.1. Two-Scale Structure Analysis. The finite element analysis should be conducted both for the CLD plate at the macroscale and the 3D periodical unit cell at the microscale. The CLD structure uses its damping mechanism based on vibratory energy dissipation through transverse shear strains induced in the viscoelastic layer, so viscoelastic layer carries only transverse shear and no normal stress when the finite element model of the CLD plate is established. In the macroscale, the viscoelastic layer is defined as an orthotropic material. Thus, the global stiffness matrix \mathbf{K} and mass matrix \mathbf{M} can be calculated by [23]

$$\mathbf{K} = \sum_{e=1}^N (\mathbf{K}_e^b + \mathbf{K}_e^v + \mathbf{K}_e^c) = \sum_{e=1}^N \left(\int_{\Omega_e} \mathbf{B}^T \mathbf{D}^b \mathbf{B} d\Omega_e + \int_{\Omega_e} (D_{55}^H \mathbf{N}_{xz}^T \mathbf{N}_{xz} + D_{44}^H \mathbf{N}_{yz}^T \mathbf{N}_{yz}) d\Omega_e + \int_{\Omega_e} \mathbf{B}^T \mathbf{D}^c \mathbf{B} d\Omega_e \right), \quad (3)$$

$$\mathbf{M} = \sum_{e=1}^N (\mathbf{M}_e^b + \mathbf{M}_e^v + \mathbf{M}_e^c) = \sum_{e=1}^N \left(\int_{\Omega_e} \rho^b \mathbf{N}^T \mathbf{N} d\Omega_e + \int_{\Omega_e} \rho^H \mathbf{N}^T \mathbf{N} d\Omega_e + \int_{\Omega_e} \rho^c \mathbf{N}^T \mathbf{N} d\Omega_e \right). \quad (4)$$

In these equations, \mathbf{K}_e^b , \mathbf{K}_e^v , \mathbf{K}_e^c , \mathbf{M}_e^b , \mathbf{M}_e^v , and \mathbf{M}_e^c are the e th element stiffness and mass matrix of the base plate, viscoelastic layer, and constrained layer, respectively. \mathbf{B} and \mathbf{N} are the strain matrix and the shape function matrix, respectively. \mathbf{D}^b , \mathbf{D}^c , ρ^b , and ρ^c are constitutive matrix and mass density of the base plate and constrained layer, respectively. ρ^H is the average mass density of the viscoelastic layer. D_{44}^H and D_{55}^H are the effective shear modulus of the viscoelastic layer. \mathbf{N}_{xz} and \mathbf{N}_{yz} are the shape function matrix of the shear strains γ_{xz} and γ_{yz} in the viscoelastic layer, respectively.

The global stiffness matrix \mathbf{K} contains the real part \mathbf{K}_R and the imaginary part \mathbf{K}_I , which are defined as follows:

$$\mathbf{K}_R = \sum_{e=1}^N (\mathbf{K}_e^b + \text{Re}(\mathbf{K}_e^v) + \mathbf{K}_e^c), \quad (5)$$

$$\mathbf{K}_I = \sum_{e=1}^N \text{Im}(\mathbf{K}_e^v), \quad (6)$$

where “Re” denotes “Real part of” and “Im” represents “Imaginary part of.”

The governing equation of the CLD structure for free vibration is written as follows:

$$\ddot{\mathbf{M}}\mathbf{X} + (\mathbf{K}_R + j\mathbf{K}_I)\mathbf{X} = 0, \quad (7)$$

where \mathbf{X} is the displacement vector in the macrostructure.

According to the Modal Strain Energy Method, the modal loss factor at the r th mode can be found as follows:

$$\eta_r = \frac{\Phi_r^T \mathbf{K}_I \Phi_r}{\Phi_r^T \mathbf{K}_R \Phi_r}, \quad (8)$$

where Φ_r is the eigenvector, which is obtained by the real modal analysis.

The effective elastic properties of the viscoelastic layer directly depend on its microstructure. In micromechanics, there are two basic theories: the homogenization theory [28–30] and the strain energy-based method [35–37]. The basic feature of the strain energy-based method is that both the unit cell of the periodic structure and the corresponding unit volume of the homogeneous solid undergo the same strain energy. Compared with the homogenization theory, the strain energy-based method can provide a relatively simple and efficient way in the estimation of the effective elastic properties and the sensitivity analysis [37].

As illustrated in Figure 1, the 3D unit cell is a cube, which does not change during the optimization process. The topology of viscoelastic damping material in a 3D unit cell is changed by varying the design variables x_i . The 3D unit cell of the viscoelastic layer is defined as an orthotropic material. The generalized Hooke’s law can be written as follows:

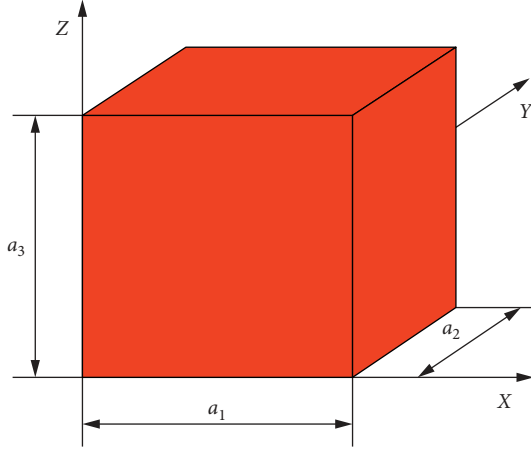


FIGURE 1: A 3D unit cell.

$$\begin{Bmatrix} \bar{\sigma}_1 \\ \bar{\sigma}_2 \\ \bar{\sigma}_3 \\ \bar{\sigma}_4 \\ \bar{\sigma}_5 \\ \bar{\sigma}_6 \end{Bmatrix} = \begin{bmatrix} D_{11}^H & D_{13}^H & D_{13}^H & 0 & 0 & 0 \\ D_{21}^H & D_{22}^H & D_{23}^H & 0 & 0 & 0 \\ D_{31}^H & D_{32}^H & D_{33}^H & 0 & 0 & 0 \\ 0 & 0 & 0 & D_{44}^H & 0 & 0 \\ 0 & 0 & 0 & 0 & D_{55}^H & 0 \\ 0 & 0 & 0 & 0 & 0 & D_{66}^H \end{bmatrix} \begin{Bmatrix} \bar{\epsilon}_1 \\ \bar{\epsilon}_2 \\ \bar{\epsilon}_3 \\ \bar{\epsilon}_4 \\ \bar{\epsilon}_5 \\ \bar{\epsilon}_6 \end{Bmatrix}, \quad (9)$$

$$E_{44}^H = \frac{1}{2} V \begin{Bmatrix} 0 \\ 0 \\ 0 \\ 1 \\ 0 \\ 0 \end{Bmatrix}^T \begin{bmatrix} D_{11}^H & D_{13}^H & D_{13}^H & 0 & 0 & 0 \\ D_{21}^H & D_{22}^H & D_{23}^H & 0 & 0 & 0 \\ D_{31}^H & D_{32}^H & D_{33}^H & 0 & 0 & 0 \\ 0 & 0 & 0 & D_{44}^H & 0 & 0 \\ 0 & 0 & 0 & 0 & D_{55}^H & 0 \\ 0 & 0 & 0 & 0 & 0 & D_{66}^H \end{bmatrix} \begin{Bmatrix} 0 \\ 0 \\ 0 \\ 1 \\ 0 \\ 0 \end{Bmatrix} = \frac{1}{2} V D_{44}^H, \quad (11)$$

where V is the volume of the unit cell.

The total strain energy can also be obtained using the domain integration of the local strain energy density in the unit cell as follows:

$$E_{44} = \frac{1}{2} \int_Y \boldsymbol{\epsilon}_4^T \mathbf{D}^{mi} \boldsymbol{\epsilon}_4 dY. \quad (12)$$

Under the boundary condition described in Table 1, the finite element equation governing the unit cell can be expressed as follows:

$$\mathbf{k}' \mathbf{u}^{(4)} = \mathbf{f}^{(4)}, \quad (13)$$

where $\mathbf{u}^{(4)}$ and $\mathbf{f}^{(4)}$ are the equivalent nodal displacement vector and force vector caused by the unit strain $\bar{\epsilon}_{(4)}$. \mathbf{k}'_i is the

real part of the global stiffness matrix of the unit cell, which is expressed as follows:

where $\bar{\sigma}_\alpha$, $\bar{\epsilon}_\beta$, and $D_{\alpha\beta}^H$ ($\alpha, \beta = 1, 2, \dots, 6$) are the effective stress tensor, strain tensor, and elastic tensor.

The effective shear modulus of the unit cell D_{44}^H and D_{55}^H can be determined by applying the following two unit strain fields:

$$\begin{aligned} \bar{\epsilon}_{(4)} &= \{0 \ 0 \ 0 \ 1 \ 0 \ 0\}^T, \\ \bar{\epsilon}_{(5)} &= \{0 \ 0 \ 0 \ 0 \ 1 \ 0\}^T. \end{aligned} \quad (10)$$

The uniform strain boundary condition is replaced with equivalent Dirichlet boundary condition in numerical implementation and the corresponding boundary conditions are resumed in Tables 1 and 2 [37]. In the tables, a_1 , a_2 , and a_3 are the sizes of the 3D unit cell in the X , Y , and Z directions, respectively.

The strain energy of the orthotropic material under the unit strain $\bar{\epsilon}_{(4)}$ can be calculated by

where \mathbf{b}_i is the strain matrix of the i th element in the unit cell. \mathbf{k}'_i is the real part of the stiffness matrix of i th element.

In finite element analysis, equation (12) can be rewritten as follows:

$$\mathbf{k}' = \sum_{i=1}^n \int_{Y_i} x_i^p \mathbf{b}_i^T \mathbf{D}^{v0} \mathbf{b}_i dY_i = \sum_{i=1}^n x_i^p \mathbf{k}'_i, \quad (14)$$

where \mathbf{b}_i is the strain matrix of the i th element in the unit cell. \mathbf{k}'_i is the real part of the stiffness matrix of i th element.

In finite element analysis, equation (12) can be rewritten as follows:

$$E_{44} = \frac{1}{2} \sum_{i=1}^n x_i^p \mathbf{u}_i^{(4)T} (1 + j\eta^0) \mathbf{k}'_i \mathbf{u}_i^{(4)}, \quad (15)$$

where $\mathbf{u}_i^{(4)}$ represents the equivalent nodal displacement vector of the i th element.

TABLE 1: Boundary conditions for the FE model of the unit cell.

Nodes	u_x	u_y	u_z
$x = 0$	0	Free	Free
$x = a_1$	0	Free	Free
$y = 0$	0	Free	0
$y = a_2$	0	Free	0
$z = 0$	0	0	Free
$z = a_3$	0	a_3	0

TABLE 2: Boundary conditions for the FE model of the unit cell.

Nodes	u_x	u_y	u_z
$x = 0$	Free	0	0
$x = a_1$	Free	0	0
$y = 0$	Free	0	Free
$y = a_2$	Free	0	Free
$z = 0$	0	0	Free
$z = a_3$	a_3	0	0

Keeping in mind that $E_{44}^H = E_{44}$, the effective shear modulus of the unit cell D_{44}^H can be expressed as follows:

$$D_{44}^H = \frac{\sum_{i=1}^n x_i^p \mathbf{u}_i^{(4)T} (1 + j\eta^0) \mathbf{k}'_i \mathbf{u}_i^{(4)}}{V}. \quad (16)$$

Similarly, the effective shear modulus of the unit cell D_{55}^H is expressed as follows:

$$D_{55}^H = \frac{\sum_{i=1}^n x_i^p \mathbf{u}_i^{(5)T} (1 + j\eta^0) \mathbf{k}'_i \mathbf{u}_i^{(5)}}{V}, \quad (17)$$

where $\mathbf{u}_i^{(5)}$ is the equivalent nodal displacement vector of the i th element, which can be obtained through the statics analysis of the unit cell under the boundary condition described in Table 2.

The constitutive matrix of an orthotropic material has nine independent components, see equation (9). The procedure for the analysis of the effective shear modulus D_{44}^H and D_{55}^H is shown in the paper, and the procedure of the identification of the other seven components can be obtained from [37].

The effective density of the unit cell is evaluated through the following relationship:

$$\rho^H = \frac{\sum_{i=1}^n \rho_i^v}{n}. \quad (18)$$

3.2. Sensitivity Analysis. An important step in finding the optimum distribution of the unit cell is to carry out sensitivity analysis in which the effect of each design variable on the modal loss factor is estimated. The sensitivity of the modal loss factor with respect to the design variables can be formulated as follows:

$$\frac{\partial \eta_r}{\partial x_i} = \frac{(\Phi_r^T \partial \mathbf{K}_I / \partial x_i \Phi_r)(\Phi_r^T \mathbf{K}_R \Phi_r) - (\Phi_r^T \partial \mathbf{K}_R / \partial x_i \Phi_r)(\Phi_r^T \mathbf{K}_I \Phi_r)}{(\Phi_r^T \mathbf{K}_R \Phi_r)^2}. \quad (19)$$

Substituting equations (5) and (6) to equation (19), equation (20) can be obtained:

$$\frac{\partial \eta_r}{\partial x_i} = \frac{(\Phi_r^T (\sum_{e=1}^N \partial(\text{Im}(\mathbf{K}_e^v)) / \partial x_i) \Phi_r)(\Phi_r^T \mathbf{K}_R \Phi_r) - (\Phi_r^T (\sum_{e=1}^N \partial(\text{Re}(\mathbf{K}_e^v)) / \partial x_i) \Phi_r)(\Phi_r^T \mathbf{K}_I \Phi_r)}{(\Phi_r^T \mathbf{K}_R \Phi_r)^2}. \quad (20)$$

Considering the definition of matrix \mathbf{K}_e^v in equation (3), the sensitivities of $\text{Im}(\mathbf{K}_e^v)$ and $\text{Re}(\mathbf{K}_e^v)$ can be formulated as follows:

$$\begin{aligned} \frac{\partial(\text{Im}(\mathbf{K}_e^v))}{\partial x_i} &= \int_{\Omega_e} \left(\frac{\partial(\text{Im}(D_{55}^H))}{\partial x_i} \mathbf{N}_{xz}^T \mathbf{N}_{xz} + \frac{\partial(\text{Im}(D_{44}^H))}{\partial x_i} \mathbf{N}_{yz}^T \mathbf{N}_{yz} \right) d\Omega_e, \\ \frac{\partial(\text{Re}(\mathbf{K}_e^v))}{\partial x_i} &= \int_{\Omega_e} \left(\frac{\partial(\text{Re}(D_{55}^H))}{\partial x_i} \mathbf{N}_{xz}^T \mathbf{N}_{xz} + \frac{\partial(\text{Re}(D_{44}^H))}{\partial x_i} \mathbf{N}_{yz}^T \mathbf{N}_{yz} \right) d\Omega_e. \end{aligned} \quad (21)$$

By analyzing the first partial derivative of equations (16) and (17) with respect to the design variables, the sensitivities of the effective shear modulus can be obtained:

$$\begin{aligned}
\frac{\partial(\text{Im}(D_{44}^H))}{\partial x_i} &= \frac{p x_i^{p-1} \eta_i^0 \mathbf{u}_i^{(4)T} \mathbf{k}'_i \mathbf{u}_i^{(4)}}{V}, \\
\frac{\partial(\text{Re}(D_{44}^H))}{\partial x_i} &= \frac{p x_i^{p-1} \mathbf{u}_i^{(4)T} \mathbf{k}'_i \mathbf{u}_i^{(4)}}{V}, \\
\frac{\partial(\text{Im}(D_{55}^H))}{\partial x_i} &= \frac{p x_i^{p-1} \eta_i^0 \mathbf{u}_i^{(5)T} \mathbf{k}'_i \mathbf{u}_i^{(5)}}{V}, \\
\frac{\partial(\text{Re}(D_{55}^H))}{\partial x_i} &= \frac{p x_i^{p-1} \mathbf{u}_i^{(5)T} \mathbf{k}'_i \mathbf{u}_i^{(5)}}{V}.
\end{aligned} \tag{22}$$

3.3. Optimization Procedure. The entire topology optimization procedure for the design of the viscoelastic material

microstructure is illustrated in Figure 2. Based on the initial microstructure, the effective shear modulus and density are computed by the homogenization process in equations (16), (17), and (18). The modal loss factor of the macrostructure and the corresponding sensitivities with respect to the design variables are calculated by a two-scale analysis in equations (8) and (20). Then, the MMA algorithm is utilized for the optimizer to update the new design variables. This process is repeated until a certain convergence criterion is satisfied. The convergence criterion is that the maximum difference of the design variables of two adjacent iteration steps is less than the given small value ε . The convergence parameter is $\varepsilon = 0.005$.

The MMA algorithm was proposed to adjust the curvature of the convex linearization method. Giving the current design $x_i^{(k)}$, the MMA approximation of the maximum modal loss factor problem in equation (1) yields to the following linear programming problem:

$$\left\{ \begin{array}{l} \text{find : } x_i, \quad i = 1, 2, \dots, n, \\ \text{min : } \sum_{i=1}^n \left[\frac{(x_i^{(k)} - L_i^{(k)})^2}{x_i - L_i^{(k)}} \frac{\partial \eta_r}{\partial x_i}(x_i^{(k)}) \right] \quad (r = 1, 2, 3, \dots, ; \quad i = 1, 2, \dots, n), \\ \text{s.t: } \frac{\sum_{i=1}^n x_i V_i}{\sum_{i=1}^n V_i} \leq V^*, \\ 0 < x_{\min} \leq x_i \leq 1, \quad i = 1, 2, \dots, n. \end{array} \right. \tag{23}$$

The lower and upper asymptotes $L_i^{(k)}$ and $U_i^{(k)}$ are iteratively updated to mitigate oscillation or improve convergence rate. The heuristic rule is as follows [22].

For $k = 1$ and $k = 2$,

$$\left\{ \begin{array}{l} U_i^{(k)} + L_i^{(k)} = 2x_i^{(k)}, \\ U_i^{(k)} - L_i^{(k)} = 1. \end{array} \right. \tag{24}$$

For $k \geq 3$,

$$\left\{ \begin{array}{l} U_i^{(k)} + L_i^{(k)} = 2x_i^{(k)}, \\ U_i^{(k)} - L_i^{(k)} = \gamma_i^{(k)}, \end{array} \right. \tag{25}$$

where

$$\gamma_i^{(k)} = \left\{ \begin{array}{l} 0.7(x_i^{(k)} - x_i^{(k-1)})(x_i^{(k-1)} - x_i^{(k-2)}) < 0, \\ 1.2(x_i^{(k)} - x_i^{(k-1)})(x_i^{(k-1)} - x_i^{(k-2)}) > 0, \\ (x_i^{(k)} - x_i^{(k-1)})(x_i^{(k-1)} - x_i^{(k-2)}) = 0. \end{array} \right. \tag{26}$$

4. Numerical Examples

Two numerical examples are presented in this section to illustrate the microstructural design of the CLD plates and demonstrate the effectiveness of the proposed optimization approach. The first is a rectangular plate with two short edges clamped and the second is a cantilever rectangular plate. It is assumed that the material properties of both cases are the same, as shown in Table 3.

It is assumed that the 3D unit cell characteristic size is much smaller than the characteristic size of the macrostructure. Such hypotheses support the homogenization theory that is used here to compute equivalent mechanical properties of the periodic viscoelastic damping materials. Then, the homogenized material properties of viscoelastic damping materials are independent of the size of the 3D unit cell [20]. For simplicity, nondimensional sizes $1 \times 1 \times 1$ for the 3D unit cell are assumed. The 3D unit cell of the microstructure is discretized with eight-node hexahedron elements. The initial designs are of a uniform distribution with the given volume fraction except the elements at the center. The density of the elements at the center is set to be 1.

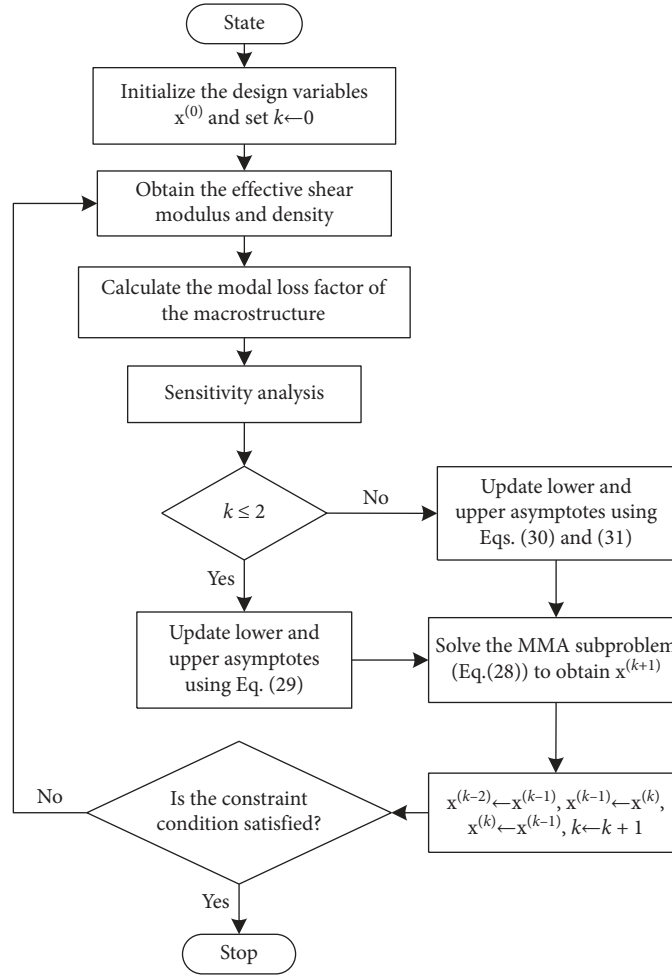


FIGURE 2: Flowchart for the optimization procedure.

TABLE 3: Physical parameters of the CLD plates.

Layer	Density (kg/m ³)	Young's modulus (MPa)	Poisson's ratio	Material loss factor
Base plate	7900	2.06×10^5	0.3	---
Viscoelastic layer	1200	40	0.49	0.5
Constrained layer	2700	7×10^4	0.3	---

4.1. The Plate Clamped with Two Short Edges. The plate clamped with two short edges is shown in Figure 3. The length and width of the cantilever rectangular plate are 0.4 m and 0.2 m, respectively. The thickness of the base plate, viscoelastic layer, and constrained layer are 0.002 m, 0.0005 m, and 0.0005 m, respectively.

Topology optimization of the microstructure is carried out first for four different meshes of the 3D unit cell: $15 \times 15 \times 15$, $20 \times 20 \times 20$, $25 \times 25 \times 25$, and $30 \times 30 \times 30$. The optimization objective is to maximize the modal loss factor of the first mode and the volume fraction is 0.3. All of the results are shown in Table 4. It can be clearly seen that the optimum objective values of the final topologies using different meshes are close to each other. With the increase of the number of elements in the 3D unit cell, the optimized configurations are more detailed, but the computation time is significantly increased. The number of elements in a 3D

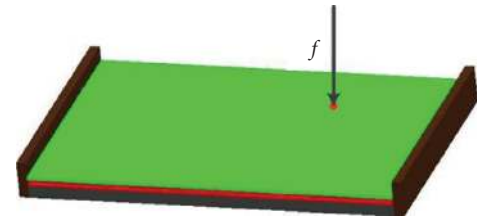


FIGURE 3: The plate clamped with two short edges.

unit cell can be determined by comprehensively considering the detail of the optimized configurations and the computational cost. The 3D unit cell in the following examples is divided into $20 \times 20 \times 20$. From Table 4, it can also be seen that the optimal configurations have very few intermediate density elements. It means that while the design variables can be fractions, most design variables are close to 0 or 1.

TABLE 4: Topological designs of viscoelastic damping material microstructures for four different meshes.

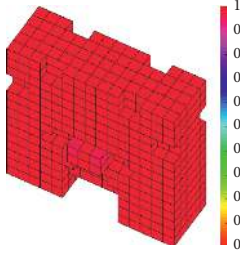
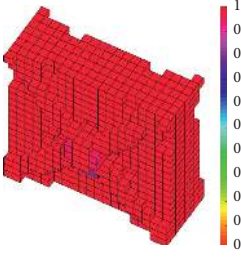
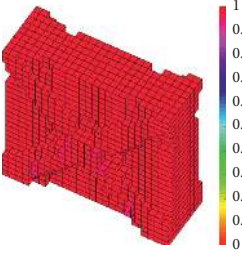
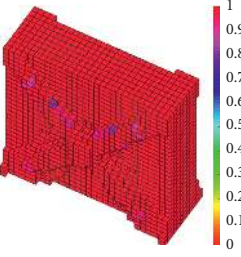
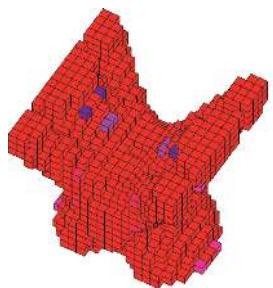
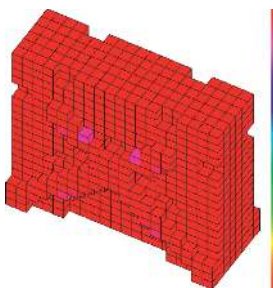
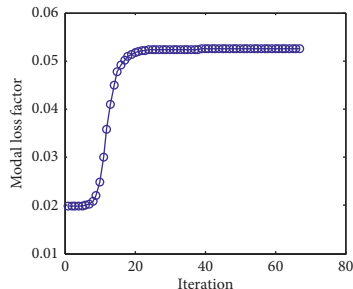
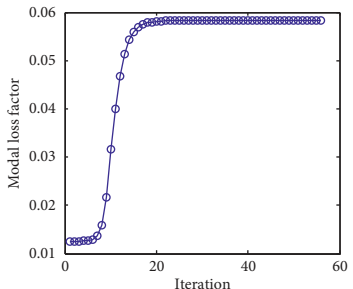
	$15 \times 15 \times 15$	$20 \times 20 \times 20$	$25 \times 25 \times 25$	$30 \times 30 \times 30$
Microstructure				
Number of iterations	51	57	77	100
Computational cost (s)	1053.94	2809.80	7615.37	17812.88
Effective storage shear modulus (MPa)	$\text{Re}(D_{44}^H) = 0.56$ $\text{Re}(D_{55}^H) = 3.77$	$\text{Re}(D_{44}^H) = 0.50$ $\text{Re}(D_{55}^H) = 3.83$	$\text{Re}(D_{44}^H) = 0.41$ $\text{Re}(D_{55}^H) = 3.80$	$\text{Re}(D_{44}^H) = 0.36$ $\text{Re}(D_{55}^H) = 3.73$
Modal loss factor	0.0648	0.0648	0.0648	0.0649

TABLE 5: Topological designs of viscoelastic damping material microstructures with the same volume fraction.

	Mode 2	Mode 3
Volume fraction	0.3	0.3
Microstructure		
Convergence histories		
Number of iterations	67	56
Computational cost (s)	3324.38	2751.62
Effective storage shear modulus (MPa)	$\text{Re}(D_{44}^H) = 1.56$ $\text{Re}(D_{55}^H) = 3.17$	$\text{Re}(D_{44}^H) = 0.49$ $\text{Re}(D_{55}^H) = 3.85$
Modal loss factor	0.0525	0.0584

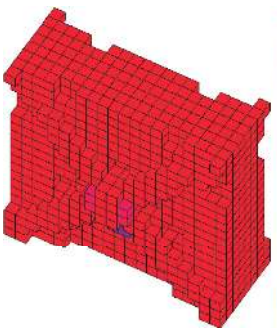
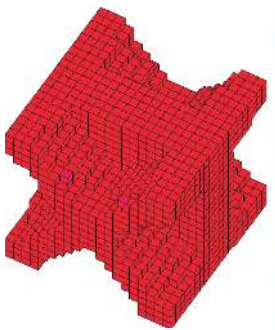
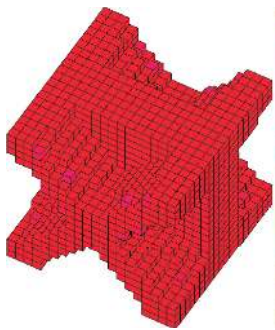
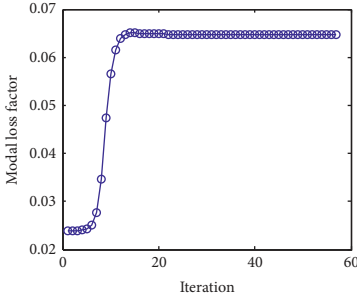
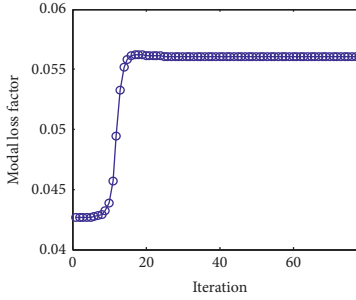
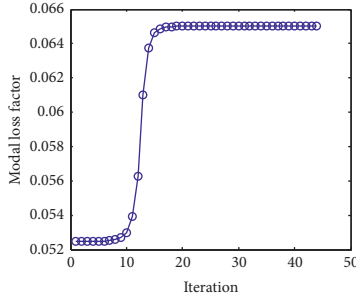
The design results of maximizing the modal loss factor of the second mode and the modal loss factor of the third mode are shown in Table 5. It is found that the optimal microstructure of maximizing the modal loss factor of the second mode is obviously different from those of maximizing the modal loss factor of the first mode and the third mode. That is because the first mode and the third mode are bending modes and the shear strains occur in the plane y - z , while the second mode is torsional mode and the shear strains occur in the planes y - z and x - z .

For each mode, there is a certain value of the shear modulus that maximizes the modal loss factor in the damping

structure. The volume fraction varies with the optimization objective. Three different design objectives are considered. They are (1) maximizing the modal loss factor of the first mode, (2) maximizing the modal loss factor of the second mode, and (3) maximizing the modal loss factor of the third mode. The design results are shown in Table 6. It can be seen that the iterations are smooth. For the single mode design, the modal loss factors of optimal designs are increased by 48.28%, 14.72%, and 6.56% than the traditional design (the solid viscoelastic material) at modes 1, 2, and 3, respectively.

In order to further verify the effectiveness of the optimal designs, the CLD plate is excited by a central time-harmonic

TABLE 6: Topological designs of viscoelastic damping material microstructures with different volume fractions.

	Mode 1	Mode 2	Mode 3
Volume fraction	0.3	0.5	0.6
Microstructure			
Convergence histories			
Number of iterations	57	80	44
Computational cost (s)	2809.80	3952.76	2181.87
Effective storage shear modulus (MPa)	$\text{Re}(D_{44}^H) = 0.50, \text{Re}(D_{55}^H) = 3.83$	$\text{Re}(D_{44}^H) = 3.77, \text{Re}(D_{55}^H) = 6.15$	$\text{Re}(D_{44}^H) = 5.29, \text{Re}(D_{55}^H) = 7.61$
Modal loss factor of optimal design	0.0648	0.0561	0.0650
Modal loss factor of traditional design	0.0437	0.0489	0.0610

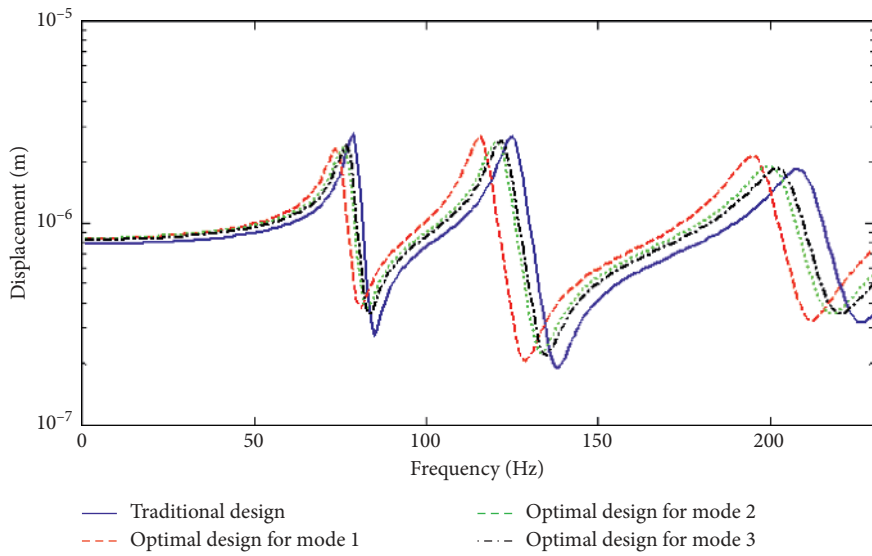


FIGURE 4: Comparison of the amplitude of frequency response function of traditional design and optimal designs.

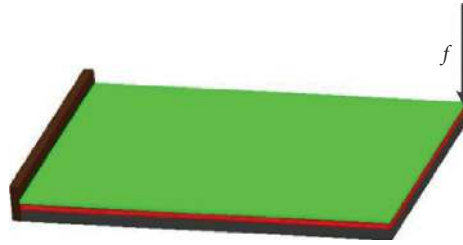
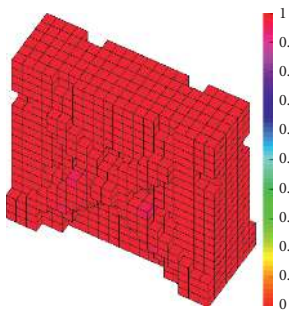
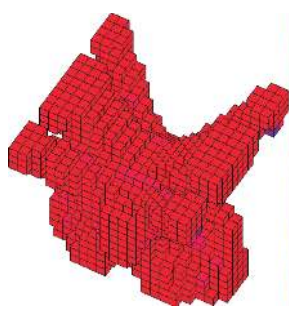
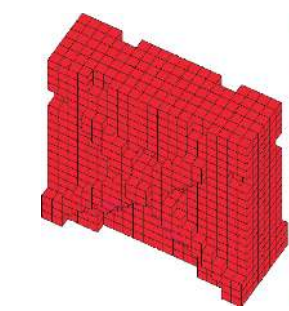
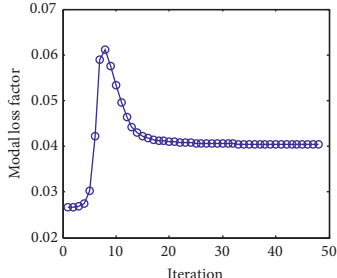
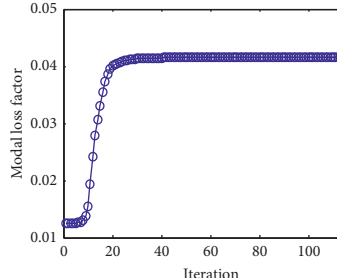
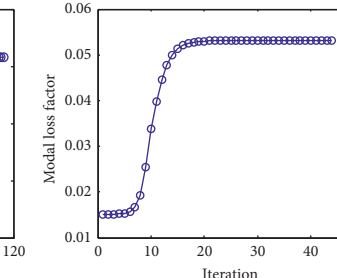


FIGURE 5: The cantilever rectangular plate.

TABLE 7: Topological designs of viscoelastic damping material microstructures with the same volume fraction.

	Mode 1	Mode 2	Mode 3
Volume fraction	0.3	0.3	0.3
Microstructure			
Convergence histories			
Number of iterations	48	116	44
Computational cost (s)	2367.75	5837.99	2163.63
Effective storage shear modulus (MPa)	$\text{Re}(D_{44}^H) = 0.49, \text{Re}(D_{55}^H) = 3.79$	$\text{Re}(D_{44}^H) = 1.50, \text{Re}(D_{55}^H) = 3.18$	$\text{Re}(D_{44}^H) = 0.49, \text{Re}(D_{55}^H) = 3.83$
Modal loss factor of optimal design	0.0402	0.0416	0.0532

force with the amplitude $F=1\text{N}$. The location of the excitation force is shown in Figure 3 and the response is evaluated at the same point. The amplitude of frequency response function of the traditional design and the optimal designs are compared in Figure 4. It can be seen that when maximizing the first modal loss factor (Case 1), the amplitude of frequency response function at the first mode is minimum. Case 2 and Case 3 show the same tendency with Case 1.

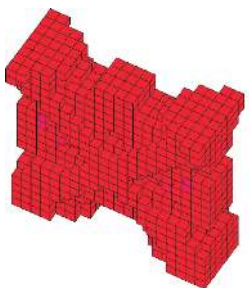
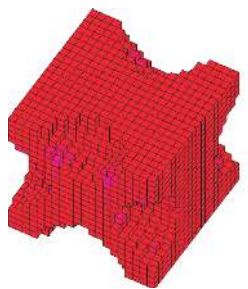
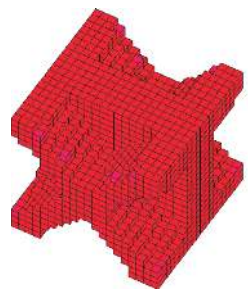
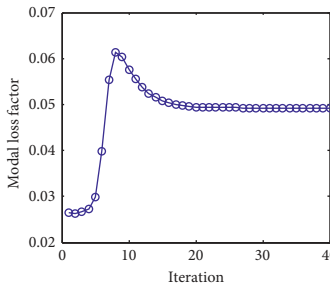
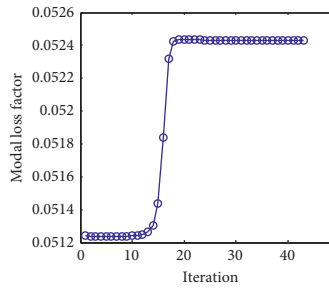
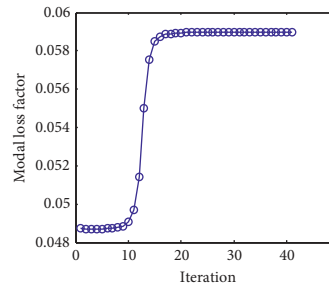
4.2. The Cantilever Rectangular Plate. In order to further verify the effectiveness of the proposed optimization algorithm, another structure with different boundary conditions and size is discussed. A cantilever rectangular plate is shown in Figure 5. The length and width of the plate are 0.2 m and 0.1 m, respectively. Other physical and geometrical parameters are the same as the first example. The volume

fraction is 0.3. Three different design objectives are considered.

The design results are shown in Table 7. Similar to the first example, the optimal microstructure and the effective shear modulus of the first mode are similar to those of the third mode. The optimal microstructure and the effective shear modulus of the second mode are obviously different from those of the first mode. That is also because the first mode and the third mode are bending modes and the shear strains occur in the plane y - z , while the second mode is the torsional mode and the shear strains occur in the planes y - z and x - z .

The volume fraction varies with the optimization objective. The design results are shown in Table 8. For the single mode design, the modal loss factors of optimal designs are increased by 160.32%, 1.55%, and 4.67% than the traditional design at modes 1, 2, and 3, respectively.

TABLE 8: Topological designs of viscoelastic damping material microstructures for maximizing modal loss factors with different volume fractions.

	Mode 1	Mode 2	Mode 3
Volume fraction	0.2	0.8	0.6
Microstructure			
Convergence histories			
Number of iterations	40	43	41
Computational cost (s)	2046.78	2352.25	2152.28
Effective storage shear modulus (MPa)	$\text{Re}(D_{44}^H) = 0.17, \text{Re}(D_{55}^H) = 2.33$	$\text{Re}(D_{44}^H) = 8.97, \text{Re}(D_{55}^H) = 10.14$	$\text{Re}(D_{44}^H) = 5.29, \text{Re}(D_{55}^H) = 7.60$
Modal loss factor of optimal design	0.0492	0.0524	0.0590
Modal loss factor of traditional design	0.0189	0.0516	0.0564

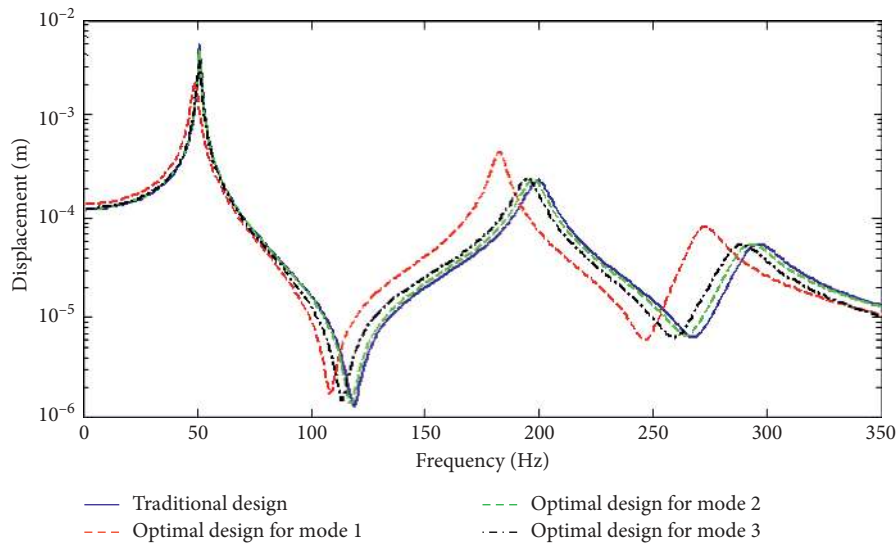


FIGURE 6: Comparison of the amplitude of frequency response function of traditional design and optimal designs.

The loading condition of frequency response analysis is similar with the first example and the location of the frequency response point is shown in Figure 5. The amplitude of frequency response function of the traditional

design and the optimal designs are compared in Figure 6. For mode 1, the resonance peak of the optimal design at the first mode is obviously lower than the traditional design. For mode 2 and mode 3, the resonance peaks of the optimal

design for the corresponding mode are slightly higher than the traditional design. This is because the stiffness of the optimal design is naturally lower than the traditional design [29].

5. Conclusions

A microstructural topology optimization of viscoelastic materials of CLD plates is presented for maximizing the modal loss factor of the macrostructure. The strain energy-based method is employed to calculate effective properties of the viscoelastic materials composed of 3D periodic unit cells. Based on the homogenized properties, the modal loss factor of the macrostructure is performed by the Modal Strain Energy Method. The design sensitivities of the modal loss factor with respect to the design variables are analyzed. The density method is adopted to find the optimum layout on microscale of the viscoelastic damping layer. The numerical examples demonstrated the effectiveness of the proposed method. The lightweight damped plates with high damping capabilities can be designed through the proposed method.

Data Availability

The data used to support the findings of this study are available from the corresponding author upon request.

Conflicts of Interest

The authors declare that they have no conflicts of interest.

Acknowledgments

This project was supported by the Natural Science Foundation of China (Grant no. 51805491), Plan of Key Research Projects of Higher Education of Henan Province (Grant no. 18A460035), and Doctoral Research Fund Project of Zhengzhou University of Light Industry (Grant no. 2015BSJJ031).

References

- [1] A. Baz, "Dynamic boundary control of beams using active constrained layer damping," *Mechanical Systems and Signal Processing*, vol. 11, no. 6, pp. 811–825, 1997.
- [2] A. L. Araújo, C. M. Mota Soares, and C. A. M. Soares, "A viscoelastic sandwich finite element model for the analysis of passive, active and hybrid structures," *Applied Composite Materials*, vol. 17, no. 5, pp. 529–542, 2010.
- [3] A. L. Araújo, P. Martins, C. M. Mota Soares, C. A. Mota Soares, and J. Herskovits, "Damping optimisation of hybrid active-passive sandwich composite structures," *Advances in Engineering Software*, vol. 46, no. 1, pp. 69–74, 2012.
- [4] R. Plunkett and C. T. Lee, "Length optimization for constrained viscoelastic layer damping," *The Journal of the Acoustical Society of America*, vol. 48, no. 1B, pp. 150–161, 1970.
- [5] M. C. Ray and A. Baz, "Optimization of energy dissipation of active constrained layer damping treatments of plates," *Journal of Sound and Vibration*, vol. 208, no. 3, pp. 391–406, 1997.
- [6] B. C. Nakra, "Vibration control in machines and structures using viscoelastic damping," *Journal of Sound and Vibration*, vol. 211, no. 3, pp. 449–466, 1998.
- [7] H. Zheng, C. Cai, G. S. H. Pau et al., "Minimizing vibration response of cylindrical shells through layout optimization of passive constrained layer damping treatments," *Journal of Sound and Vibration*, vol. 279, no. 3–5, pp. 739–756, 2005.
- [8] M. P. Bendsoe and N. Kikuchi, "Generating optimal topologies in structural design using a homogenization method," *Computer Methods in Applied Mechanics and Engineering*, vol. 71, no. 2, pp. 197–224, 1988.
- [9] M. P. Bendsoe, "Optimal shape design as a material distribution problem," *Structural Optimization*, vol. 1, pp. 193–202, 1989.
- [10] M. Y. Wang, X. Wang, and D. Guo, "A level set method for structural topology optimization," *Computer Methods in Applied Mechanics and Engineering*, vol. 192, no. 1–2, pp. 227–246, 2003.
- [11] Y. M. Xie and G. P. Steven, "A simple evolutionary procedure for structural optimization," *Computers & Structures*, vol. 49, no. 5, pp. 885–896, 1993.
- [12] X. Y. Yang, Y. M. Xie, G. P. Steven, and O. M. Querin, "Bidirectional evolutionary method for stiffness optimization," *AIAA Journal*, vol. 37, no. 11, pp. 1483–1488, 1999.
- [13] S. Y. Kim, C. K. Mechefske, and I. Y. Kim, "Optimal damping layout in a shell structure using topology optimization," *Journal of Sound and Vibration*, vol. 332, no. 12, pp. 2873–2883, 2013.
- [14] K. A. James and H. Waisman, "Topology optimization of viscoelastic structures using a time-dependent adjoint method," *Computer Methods in Applied Mechanics and Engineering*, vol. 285, pp. 166–187, 2015.
- [15] J. F. A. Madeira, A. L. Araújo, and C. M. Mota Soares, "Multiobjective optimization of constrained layer damping treatments in composite plate structures," *Mechanics of Advanced Materials and Structures*, vol. 24, no. 5, pp. 427–436, 2017.
- [16] O. Sigmund, "Materials with prescribed constitutive parameters: an inverse homogenization problem," *International Journal of Solids and Structures*, vol. 31, no. 17, pp. 2313–2329, 1994.
- [17] O. Sigmund, "Tailoring materials with prescribed elastic properties," *Mechanics of Materials*, vol. 20, no. 4, pp. 351–368, 1995.
- [18] Y.-M. Yi, S.-H. Park, and S.-K. Youn, "Design of microstructures of viscoelastic composites for optimal damping characteristics," *International Journal of Solids and Structures*, vol. 37, no. 35, pp. 4791–4810, 2000.
- [19] X. Huang, S. Zhou, G. Sun, G. Li, and Y. M. Xie, "Topology optimization for microstructures of viscoelastic composite materials," *Computer Methods in Applied Mechanics and Engineering*, vol. 283, no. 253, pp. 503–516, 2015.
- [20] Q. Liu, D. Ruan, and X. Huang, "Topology optimization of viscoelastic materials on damping and frequency of macrostructures," *Computer Methods in Applied Mechanics and Engineering*, vol. 337, pp. 305–323, 2018.
- [21] O. Sigmund, "On the usefulness of non-gradient approaches in topology optimization," *Structural and Multidisciplinary Optimization*, vol. 43, no. 5, pp. 589–596, 2011.
- [22] K. Svanberg, "The method of moving asymptotes—a new method for structural optimization," *International Journal for*

- Numerical Methods in Engineering*, vol. 24, no. 2, pp. 359–373, 1987.
- [23] L. Zheng, R. Xie, Y. Wang, and E.-S. Adel, “Topology optimization of constrained layer damping on plates using method of moving asymptote (MMA) approach,” *Shock and Vibration*, vol. 18, no. 1-2, pp. 221–244, 2011.
- [24] Z. Kang, X. Zhang, S. Jiang, and G. Cheng, “On topology optimization of damping layer in shell structures under harmonic excitations,” *Structural and Multidisciplinary Optimization*, vol. 46, no. 1, pp. 51–67, 2012.
- [25] A. El-Sabbagh and A. Baz, “Topology optimization of unconstrained damping treatments for plates,” *Engineering Optimization*, vol. 46, no. 9, pp. 1153–1168, 2014.
- [26] A. Takezawa, M. Daifuku, Y. Nakano, K. Nakagawa, T. Yamamoto, and M. Kitamura, “Topology optimization of damping material for reducing resonance response based on complex dynamic compliance,” *Journal of Sound and Vibration*, vol. 365, pp. 230–243, 2016.
- [27] Z. Fang, J. Hou, and H. Zhai, “Topology optimization of constrained layer damping structures subjected to stationary random excitation,” *Shock and Vibration*, vol. 2018, Article ID 7849153, 9 pages, 2018.
- [28] W. Chen and S. Liu, “Microstructural topology optimization of viscoelastic materials for maximum modal loss factor of macrostructures,” *Structural and Multidisciplinary Optimization*, vol. 53, no. 1, pp. 1–14, 2016.
- [29] K.-S. Yun and S.-K. Youn, “Microstructural topology optimization of viscoelastic materials of damped structures subjected to dynamic loads,” *International Journal of Solids and Structures*, vol. 147, pp. 67–79, 2018.
- [30] J. Zhao, H. Yoon, and B. D. Youn, “Concurrent topology optimization with uniform microstructure for minimizing dynamic response in the time domain,” *Computers & Structures*, vol. 222, pp. 98–117, 2019.
- [31] M. P. Bendsøe and O. Sigmund, “Material interpolation schemes in topology optimization,” *Archive of Applied Mechanics*, vol. 69, pp. 635–654, 1999.
- [32] Y. Du, S. Yan, Y. Zhang, H. Xie, and Q. Tian, “A modified interpolation approach for topology optimization,” *Acta Mechanica Solida Sinica*, vol. 28, no. 4, pp. 420–430, 2015.
- [33] Y. Kun, C. G. Dong, and W. B. Ping, “Topology optimization of damping layers in shell structures subject to impact loads for minimum residual vibration,” *Journal of Sound and Vibration*, vol. 431, pp. 226–247, 2018.
- [34] H. Zhang, X. Ding, H. Li, and M. Xiong, “Multi-scale structural topology optimization of free-layer damping structures with damping composite materials,” *Composite Structures*, vol. 212, pp. 609–624, 2019.
- [35] E. J. Barbero, *Finite Element Analysis of Composite Material*, Taylor and Francis Group, Milton Park, UK, 2008.
- [36] W. Zhang, G. Dai, F. Wang, S. Sun, and H. Bassir, “Using strain energy-based prediction of effective elastic properties in topology optimization of material microstructures,” *Acta Mechanica Sinica*, vol. 23, no. 1, pp. 77–89, 2007.
- [37] A. Catapano and M. Montemurro, “A multi-scale approach for the optimum design of sandwich plates with honeycomb core. Part I: homogenisation of core properties,” *Composite Structures*, vol. 118, pp. 664–676, 2014.